Title

Active scour monitoring using ultrasonic time-domain reflectometry to detect a soil interface

Authors

Funderburk, Morgan L
Todd, Michael D
Netchaev, Anton
et al.

Publication Date

2021-03-31

DOI

10.1117/12.2582457

Peer reviewed

Active Scour Monitoring using Ultrasonic Time-Domain Reflectometry to Detect a Soil Interface

Morgan L. Funderburk[a,b], Michael D. Todd[a], Anton Netchaev[c], and Kenneth J. Loh[a,b,*]

[a] Department of Structural Engineering, University of California San Diego, La Jolla, CA 92093-0085, USA;

[b] Active, Responsive, Multifunctional, and Ordered-materials Research (ARMOR) Lab, University of California San Diego, La Jolla, CA 92093-0085, USA;

[c] U.S. Army Engineer Research and Development Center, U.S. Army Corp of Engineers, Vicksburg, MS 39180, USA.

ABSTRACT

Local scour is arguably the most pressing issue regarding the safety and longevity of overwater civil infrastructure. Many modern scour detection techniques do not provide continuous scour depth measurements, nor can they function under extreme flow conditions, which is when scour monitoring becomes most critical. Thus, the objective of this study was to develop scour depth monitoring sensors using ultrasonic time domain reflectometry (UTDR). The scour sensor was based on an aluminum strip with two piezoelectric macro fiber composites (MFCs) bonded at one end. The aluminum strip or rod-like sensor is intended to be driven and buried at the location where scour depth measurements are desired. The two MFCs were used to either generate or sense ultrasonic Lamb wave pulses propagating in the aluminum strip. During scour, as sediment is eroded from around the base of the strip, the distance (*i.e.*, scour depth) between the MFCs and the soil interface would increase. The hypothesis was that increasing scour depth would change the mechanical impedance of the system to cause measurable and unique signatures in the residual Lamb wave signals. To test this hypothesis, different interfaces (*i.e.*, metal-metal, polymer-metal, and soil-metal) were applied at different locations along the aluminum strip and MFC system. The MFC sensor-actuator pair was actuated to propagate and measure the corresponding Lamb waves during each test. The results showed clear changes in the residual signal, which were well-correlated to the changing locations of the artificial interface. In particular, the time-of-flight of the response pulse within the residual signature could be used to accurately determine the location of the soil interface or scour depth. Overall, this study demonstrated feasibility of an UTDR sensor for scour monitoring.

Keywords: Lamb wave, macro fiber composite, piezoelectric, scour monitoring, ultrasonic, UTDR

1. INTRODUCTION

Between 1992 and 2014, hydraulic failure – failures recorded with descriptions such as hydraulic, flood, scour, tidal, and debris – was found to be the cause of over 55% of all bridge collapses[1]. In addition, it was found that most hydraulic collapses were a result of scour-induced failure[2,3]. Local scour around an obstruction, such as a bridge pier, occurs when fluid downflow at the face of the obstruction induces vortices that erode sediments at its base, which jeopardizes the integrity and load-carrying capacity of the foundation[4] (Fig. 1). This phenomenon is not just limited to the U.S.; similar impacts of catastrophic scour failures have been reported worldwide[5].

Unfortunately, scour severity is often underestimated in bridges, partially because accurate measurements of scour depth underwater are difficult to obtain or are only possible during favorable weather and water conditions. An early method to monitor bridge scour was to rely on manual technicians using physical probes[2]. Undoubtably, there are major drawbacks to physical probing, including the infrequent measurement periods and the need for an on-site technician. Boat or raft sonar can map full scour topography but, again, requires a technician and is done infrequently. Float out devices, which are buried underwater and beneath soil, rise to the surface when their location is breached. These devices eliminated the need for a technician, but the sensors need to be reburied after each exposure event, which is cumbersome and expensive[6].

* Corresponding author e-mail: kenloh@ucsd.edu; phone: +1 (858) 822-0431; fax: +1 (858) 534-1310; armor.ucsd.edu

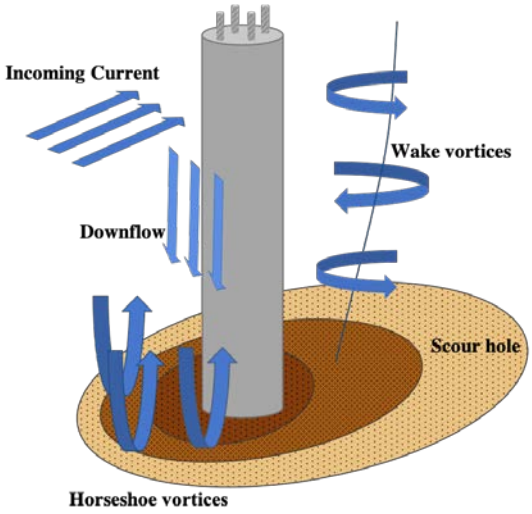

Figure 1. Local scour near bridges occurs due to the obstruction in flow caused by the bridge pier. Sediment is eroded by vortices near the base of the pier and leaves the superstructure vulnerable to damage or failure.

Continuous sonar monitoring emerged as an alternative to physical probing and float out devices. Near-bridge sonar can semi-continuously capture the critical maximum scour depth without an on-site technician. However, sonar does not function well under extreme river conditions, when entrained air and sediments would obscure the reflected sonar waves[7]. As mentioned earlier, the most critical time for measuring scour depth is during extreme flow conditions, yet this is also when sonar is least reliable. Scour holes are at their deepest during high-flow and can be filled in with less supportive soil after the high-flow period subsides[8]. Therefore, a lack of monitoring during extreme flow events would underestimate the severity of the true maximum scour depth in the monitored area and, furthermore, could overestimate the soil-support provided to the superstructure. In the retrospective by Montalvo *et al.*[1], it was found that only 17% of hydraulicly collapsed bridges were identified as scour critical before failure.

Optical sensors are one solution for mitigating the environmental effects that make detecting scour during high-flow events challenging. Optical sensors used for scour depth identification employ fiber-optic Bragg grating (FBG) sensing regions, which are microstructures within an optical fiber engineered to be sensitive to strain based on shifts in the reflected central wavelength. Mechanisms for detecting scour utilizing FBG sensors vary widely, with some detecting shifts in strain at descrete locations due to water temperature[9], water exposure[10,11], or lateral soil pressure[12]. Other methods use FBGs to monitor changes to a driven-rod;s sensing structure, either by detecting increasing levels of strain[9] or shifts in vibration frequency as scour erosion increases exposed length[13]. FBGs offer some advantages over other methods, like the ability to multiplex and an invulenrability to electrical interference. However the cost of an FBG monitoring system is prohibitive, and many mechansims only offer depth measurements at discrete locations. Futhermore, scour sensors based on the structural analysis of driven-rods are sensitive to flow-velocity and must be calibrated for soil support at each installed location[14,15].

An emerging technology proposes using time domain reflectometry (TDR) to continuously detect the soil-water interface. Current TDR methods used for bridge scour monitoring, such as electrical time domain reflectometry (ETDR), send an electromagnetic (EM) pulse down a buried conductor[16–19]. A change in the conductor's surrounding material, such as at a soil-water interface, creates a shift in electrical impedance that sends a portion of the EM pulse back to the ETDR receiver. By tracking the time-of-flight from the interface reflection, soil depth (*i.e.*, scour depth) can be determined. ETDR has the advantage of being minimally influenced by outside environmental factors, which do not cause the sensor's electrical impedance to shift suddenly. Initially, ETDR had drawbacks in that it was not easily deployable, experienced sensor fowling, and had measurement limitations due to attenuation. Improvements have been made to ETDR to develop a more robust system, which uses a bundled sensing cable to improve durability while maintaining sensitivity[20]. However, ETDR sensors still faces issues with pull-out failure due to insufficient bottom anchorage and electrical shorts due to abrasion of its insulative polymer coating[21]. Therefore, this paper aims to address the limitations of ETDR by proposing a new sensing mechanism for detecting scour using TDR, which has shown to be an accurate technique for detecting the soil-water interface without substantial environmental interference.

Ultrasonic time domain reflectometry (UTDR) has long been utilized for nondestructively detecting and locating damage in structures, such as cracks, corrosion, and composite delamination[22–24]. In particular, propagating Lamb waves have been shown to be optimal for damage detection in thin plates[25,26]. There are a variety of ways to introduce Lamb waves into a structure, but most generally they are introduced by a piezoelectric device applied at an angle to the surface of interest[27]. However, macro-fiber composites (MFCs) can also introduce Lamb waves, are highly durable, and can be easily bonded to the structure of interest[28,29]. The main limitation of MFCs is that, for most thin plates, the excitation signals fall well below the frequency needed to introduce higher order symmetric or asymmetric modes. However, the introduction of only one Lamb wave mode into a structure has been shown to be ideal for inducing clear response signals without dispersion[27]. Low frequency Lamb waves can also propagate over longer distances, which makes them ideal for long range inspections, such as for a large scour hole. In this study, Lamb waves were employed for UTDR because they disrupt both surfaces of a thin-plate, making them a prime candidate to show a potential interaction with surrounding materials[30]. Theoretically, an external constraint on the propagating material containing the Lamb wave could cause an energy reflection at the site of the constraint due to a mechanical impedance change. Therefore, first-order symmetric (S0) Lamb waves generated by MFCs were investigated for use in an UTDR sensing mechanism to detect soil-interfaces for the purposes of scour monitoring.

2. EXPERIMENTAL DETAILS

2.1 UTDR Sensor Design

A thin, long, rod-like scour sensor in the form of an aluminum strip was proposed, and the sensor could be buried and driven into the soil where scour depth measurements are desired. Two M8514-P2 MFCs from Smart Material were bonded on the same end and face of a 6 ft (1.8 m) long aluminum strip using double-sided tape (Fig. 2). One MFC acted as the actuator, while the other served as the sensor, so that an ultrasonic pulse-echo system was realized. The actuating MFC was excited using a multi-cycle Gaussian sine wave packet pulsed intermittently. The sensing MFC received the first pass of the input pulse, as well as a series of pulses reflected from impedance changes along the aluminum strip and from the end of the beam. For the experiments performed in this study, localized pressurized areas were introduced to the sensor strip using a buffered weight and various material interfaces, which will be explained in Sections 2.4 and 2.5 (Fig. 2).

2.2 Waveform Generation and Data Acquisition

As mentioned in Section 2.1, a pulse-echo setup with a pair of MFCs was implemented for the scour rod sensor. The MFC actuator was connected to an Agilent 33220A Function Waveform generator that outputted a +/- 9.5 V, 8-cycle, Gaussian sine wave pulse at a packet frequency of 2.8 kHz, giving it an overall center frequency of approximately 22 kHz. The appropriate center frequency was determined by incrementally adjusting the packet frequency and selecting the frequency that produced the largest reflected response. The EM pulse was generated every 20 ms, which gave ample time for the reflections from the previous pulse to cease. The sensing MFC was connected to a Keysight InfiniiVision DSOX3024T oscilloscope, and the outputted waveform was averaged 10x. For all the experiments performed in this study, the aluminum strip was laid flat on a hard surface so as not to induce any unwanted strain into the strip. It should be mentioned that, to

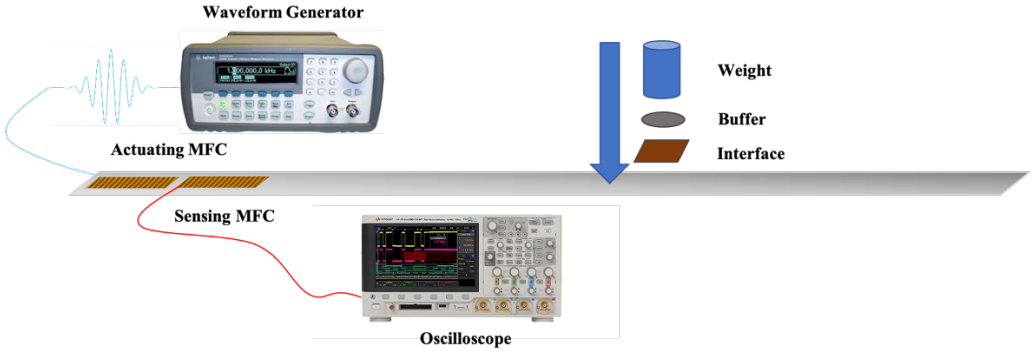

Figure 2. Two MFCs were installed to form a pulse-echo setup at one end of a 6 ft long aluminum strip. Weights were applied to the aluminum strip with a buffer to keep the pressurized area constant. The experiments performed included an additional interface layer below the buffer.

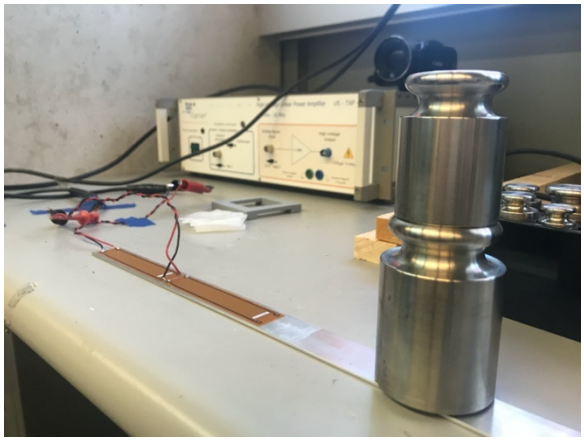

Figure 3. Pressure was applied with a metal-metal interface at different positions along the strip by placing various amounts of weight on the constant buffer area.

confirm that there was no unwanted interference from the surface, a preliminary test was performed with the strip suspended vertically mid-air; there was no notable change in the reflected waveforms between the air test and the surface test.

2.3 Velocity and Wave Mode

An ultrasonic pitch-catch test was performed to confirm the type of ultrasonic wave being generated and to determine the precise velocity of the Lamb wave. Lamb wave speed can vary based on the propagating material, material thickness, wave mode number, wave type (*i.e.*, symmetric or asymmetric), and the wave frequency. With the MFC actuator fixed at one end of the 1/16" (1.6 mm) thick aluminum strip, the MFC sensor was moved to multiple locations along its length to create different interrogation distances. Velocity was determined by taking an average of many interrogation distances divided by their corresponding times-of-arrival. Furthermore, both faces of the strip were evaluated at the same locations to determine wave mode. The actuation frequency of the MFC produced the lowest symmetric mode (S0) Lamb wave that propagated along the length of the strip. These tests showed that the S0 Lamb wave was traveling at 16,400 ft/s (5,000 m/s). This velocity was then used to calculate the corresponding location of the response waveforms. Frequency-thickness curves confirmed the mode and velocity of a Lamb wave expected at 22 kHz for an aluminum plate of this thickness. No significant dispersion of the Lamb wave was observed.

2.4 Metal-Metal Interface with Varied Pressure

Metal-metal interface testing was conducted to determine if the S0 Lamb wave could be reflected by a non-damaging pressure interface and furthermore if the time-of-flight could be used to determine the precise location of that applied pressure. Steel weights were placed on the top face of the aluminum strip, which was the same face that the MFCs were bonded to (Fig. 3). The weights range from 0.22 to 3.30 lb (100 to 1,500 g) and have varied cross-sectional base areas, so a buffer plate (washer) was employed to impart a consistent contact area between the weight and aluminum strip. Before pressure testing began, a baseline Lamb wave response signal was recorded without pressure applied to the strip. The buffered weights were then placed at 1 ft (30.5 cm) increments from 1 to 5 ft (0.35 to 1.5 m), and a residual signal (with respect to the baseline) was calculated for each location.

2.5 Metal-Polymer and Metal-Soil Interfaces

Additional tests were performed to investigate the influence of the material interface of applied pressure on the reflected wave-packet energy. Particularly of interest was the capability of UTDR to capture a substantial reflection from a metal-soil interface, as this is the mechanism which would be used for monitoring scour. The tests that were conducted followed the procedure outlined in Section 2.4. The interface study was performed using a 3.30 lb weight placed on the buffer plate. The buffer plate was then separated from the aluminum strip using two types of interfaces, namely (1) Dragon Skin (*i.e.*, a silicone elastomer molded to the desired thickness) and (2) wetted sand pressed into a 3D-printed mold. Before interface testing began, a baseline signal was also obtained. The interface weights were then placed at 1 ft increments from 1 to 5 ft, and a residual signal was calculated for each location.

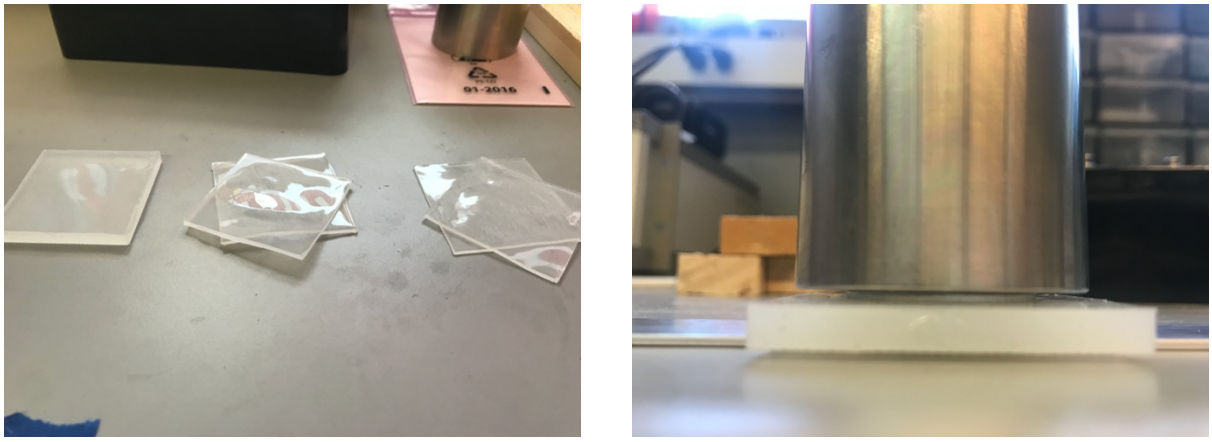

(a) (b)

Figure 4. (a) Different thicknesses of a flexible Dragon Skin elastomer film were (b) placed beneath the weights and buffer along the length of the aluminum strip.

(a) (b)

Figure 5. (a) A small hollow frame was 3D-printed to contain soil atop the aluminum strip. (b) Weights were placed on top of the soil avoiding contact with the frame.

First, Dragon Skin testing was performed with three different thicknesses of the elastomer at the interface (Fig. 4). Films with thicknesses of 0.04, 0.08, and 0.2 in (1, 2, and 5 mm) were prepared by curing the two-part polymer in their respective 3D-printed molds after mixing. The films were then used to create five unique thicknesses by stacking the films in different combinations. Second, soil interface testing was performed using a layer of wetted sand. The sand was contained in a customized 3D-printed mold designed to hold the soil in an even layer without coming into direct contact with the metal strip (Fig 5a). A small bridge allowed the aluminum strip to run through-and-through which allowed soil to escape slightly around the edges. Wetting the soil gave it enough cohesion to compact densely and stay mostly within the frame. Weights were then stacked atop the buffer on the surface of the compacted sand to apply pressure (Fig. 5b).

3. RESULTS AND DISCUSSION

The residual signals were calculated for each series of the weighted tests discussed in Sections 2.4 and 2.5. The residual signal was calculated as the difference between the weighted signal and the baseline signal (*i.e.*, the recorded signal when no weight was applied). Changes in temperature, which can add noise to the residual signal, were not considered, since stable laboratory conditions were assumed. In this work, residual signal time histories are plotted with voltage on the *y*-

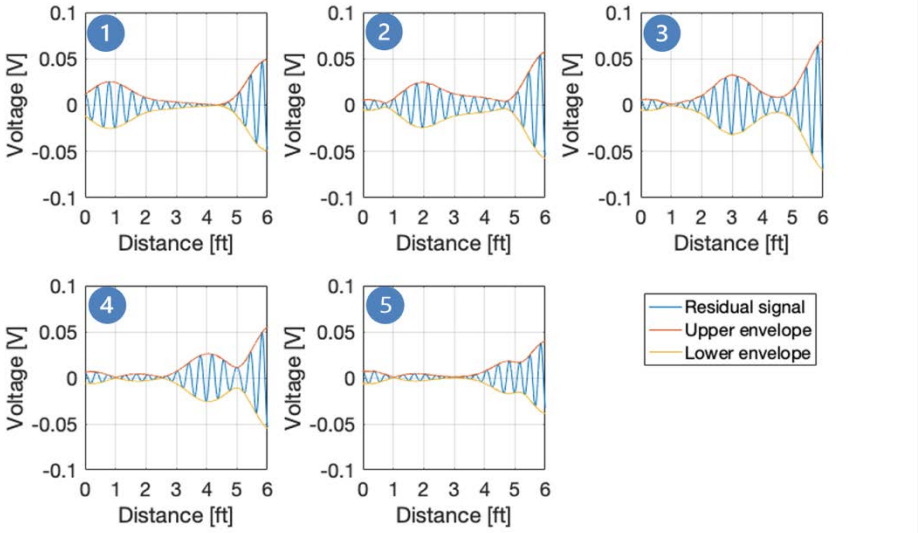

Figure 6. The residual signals collected from the MFC show a reflected wave-packet as 3.30 lb of weights are moved along the aluminum strips' length in 1ft increments. The blue numbers correspond to the positioning of the weight in 1 ft increments (*e.g.*, number 4 had the weights positioned at 4 ft). The distance on the *x*-axis was calculated by multiplying the measured time by the speed of the Lamb waves in aluminum.

axis and distance on the *x*-axis. Here, distance is given as distance from the MFC actuator and is calculated by multiplying the time-of-flight by velocity (determined in Section 2.2) and then dividing the overall distance in half due to the pulse-echo setup. Distance ranges from 0 to 6 ft, with 0 ft being the approximate location of the midline of the MFC actuator and 6 ft being the end of the aluminum strip. The blue number in each figure corresponds to the position (in ft) of the applied pressure interface.

By evaluating the residual signal, changes due to the presence of the pressurized interface could be clearly seen and analyzed. If there was no interaction with a particular pressurized interface, the residual signal would be approximately 0, regardless of the location of the applied pressure interface. The presence of residual pulses occurring between 0 and 6 ft would indicate a reflection from the pressurized interface, followed by a subsequent energy difference in the pulse due to the Lamb wave reflection from the end of the 6 ft aluminum strip. A relatively large reflection would indicate that there was more interaction between the Lamb wave and the particular pressurized interface.

3.1 Metal-Metal Interface Results

As mentioned in Section 2.4, weights were applied at different positions on the aluminum strip. The residual signals for the largest applied pressure (*i.e.*, 3.30 lb) are plotted in Fig. 6, and each plot shows two distinct reflections for each location along the length of the aluminum strip. The occurrence of the first return pulse is well-correlated with its corresponding applied pressure location, especially at locations from 1 to 4 ft. For the 5 ft case, a slight malignment in the peak of the response pulse occurs, which was likely due to interference with the second return pulse reflecting from the end of the aluminum strip. However, there is still a notable return pulse, cojoined with the end reflection, with a peak at approximately 4.75 ft. On the other hand, Fig. 6 shows that the second pulse, induced by Lamb wave reflecting from the end of the aluminum strip, appears distinctly and generates a strong residual signal regardless of where the weight was placed.

Fig. 7 shows a comparison of the peak voltages of the first response pulses (*i.e.*, the pulses returning from the pressurized interface) for all seven different weights applied. Pulses from the 1 ft location were excluded from the comparison, because residual signal peaks could not be identified when lower pressures were applied; signals from the 5 ft case were also excluded because of their interaction with the return pulse. In general, the results show a reduction in return energy as the amount of pressure was reduced, albeit with some inconsistencies potentially due to experimental and random errors. In fact, a major source of error between tests may be slight changes in the MFC bonding condition or variations in placement of the weights. Although each set of residual signals is not shown, all the residual signals showed a visible response pulse

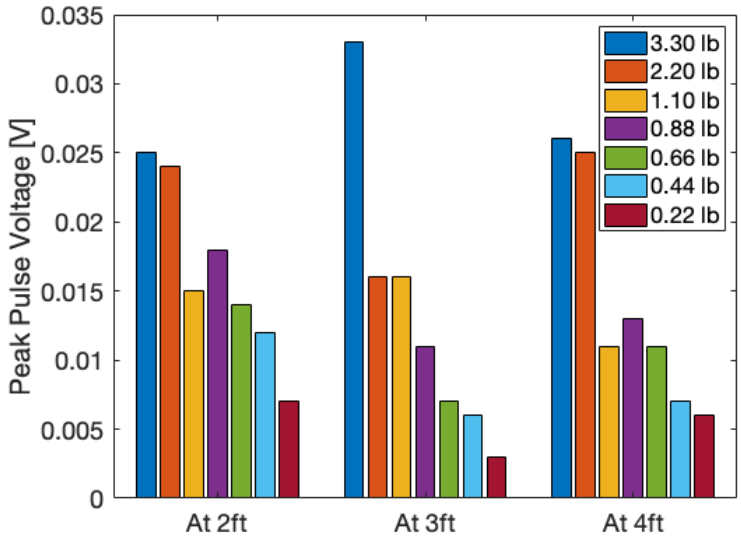

Figure 7. The peak voltages from the return wave-packet, which is related to the energy reflected, at various locations show a downward trend as the applied pressure at each location was decreased.

corresponding to the location of the pressurized interface for the 2 to 4 ft locations, as well as a end-reflection pulse at 6 ft.

3.2 Metal-Polymer Interface Results

Section 2.5 discussed how the metal-metal interface was modified to accommodate different thickness Dragon Skin elastomers to create a metal-polymer interface. Fig. 8 shows the residual signals obtained when the thinnest Dragon Skin film (*i.e.*, 0.04 in thick) was employed. Similar to Fig. 6, each residual signal in Fig. 8 shows at least two distinct pulses,

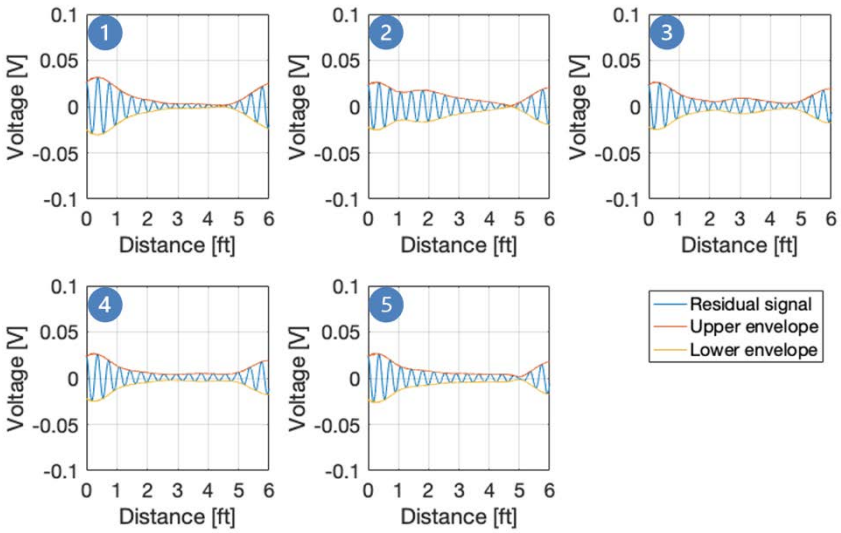

Figure 8. The residual signals show a reflected wave packet as a 3.30 lb weight – with a Dragon Skin interface – was moved along the aluminum strip's length in 1 ft increments. The distance on the *x*-axis was calculated by multiplying the measured time by the speed of the Lamb wave in aluminum.

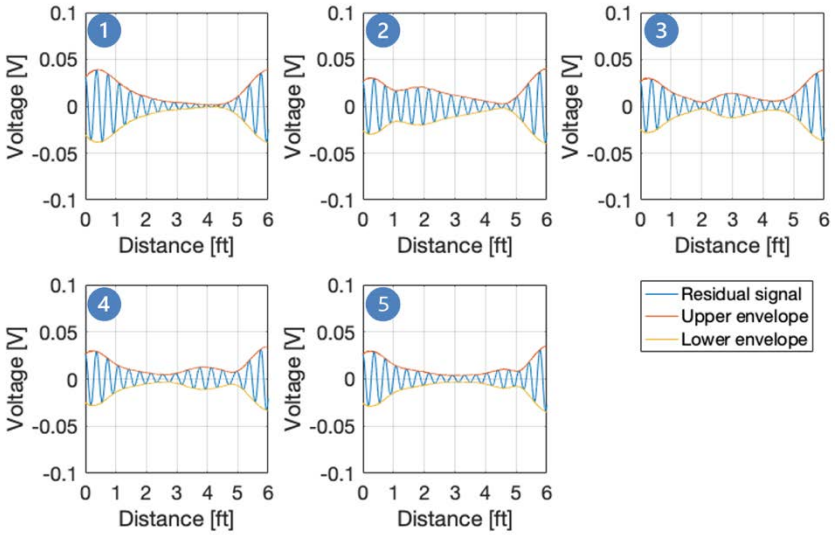

Figure 9. The residual signals show a reflected wave packet as a 3.30 lb weight – with a soil interface – was moved along the aluminum strip's length in 1 ft increments.

while some show three. The first pulse occurred slightly after the 0 ft mark, and this location corresponds approximately to the midpoint of the MFC sensor just below the MFC actuator. The appearance of this feature in the residual signal indicated that there was likely debonding occurring between either the MFC actuator or sensor or possibly both. Poor actuator/sensor contact would alter the amount of energy delivered to the system. However, it was difficult to eliminate this error (besides permanently bonding the MFCs to the aluminum strip), because debonding could happen at any point during testing, even between the collection of the baseline and the following test. Future tests will consider bonding the MFCs to the aluminum strip using a suitable epoxy.

The second residual signal feature was present only distinctly in the 2 and 3 ft locations and corresponds to the return pulse from the pressurized metal-polymer interface. No distinct return pulses appeared at 1 and 5 ft. There was a slight maximum occurring around 4 ft, but it was not as apparent as the features observed during the metal-metal interface tests (Fig. 6). The third pulse was the return pulse corresponding to the end of the aluminum strip, which was also observed in Fig. 6. A comparison of residual signals from tests performed with the same pressure (*i.e.*, 3.30 lb on a buffer plate) showed that there was no notable change in return wave-packet energy when different thicknesses of Dragon Skin was used.

3.3 Metal-Soil Interface Results

The metal-polymer interface was replaced with a metal-soil interface as was discussed in Section 2.5. A representative set of residual signals from the metal-soil interface tests is plotted in Fig. 9. Like the signals seen from the metal-polymer interface, there appear to be three distinct pulses. The first and last residual signal features correspond to the midline of the MFC sensor and the end of the beam, respectively, as was also discussed in Section 3.2. The center pulse was due to the 3.30 lb weight being applied at the 2, 3, 4, and 5 ft positions.

3.4 Interpretation and Comparison of Results

Overall, the results indicated that the first symmetric mode (S0) Lamb wave was able to be reflected from mechanical impedance changes induced by changing the boundary conditions along the aluminum strip. This means that Lamb waves could be used to detect surface condition changes (*e.g.*, due to scour) even if they do not cause permanent damage in the structure (*i.e.*, aluminum strip). The results also showed that the amount of reflected energy (*i.e.*, the peak pulse voltage) from an S0 Lamb wave is sensitive to both the amount of pressure and the type of interface applied, as was presented in Sections 3.1 to 3.3. In general, a higher pressure caused a relatively larger reflection, while a lower pressure caused a relatively smaller reflection.

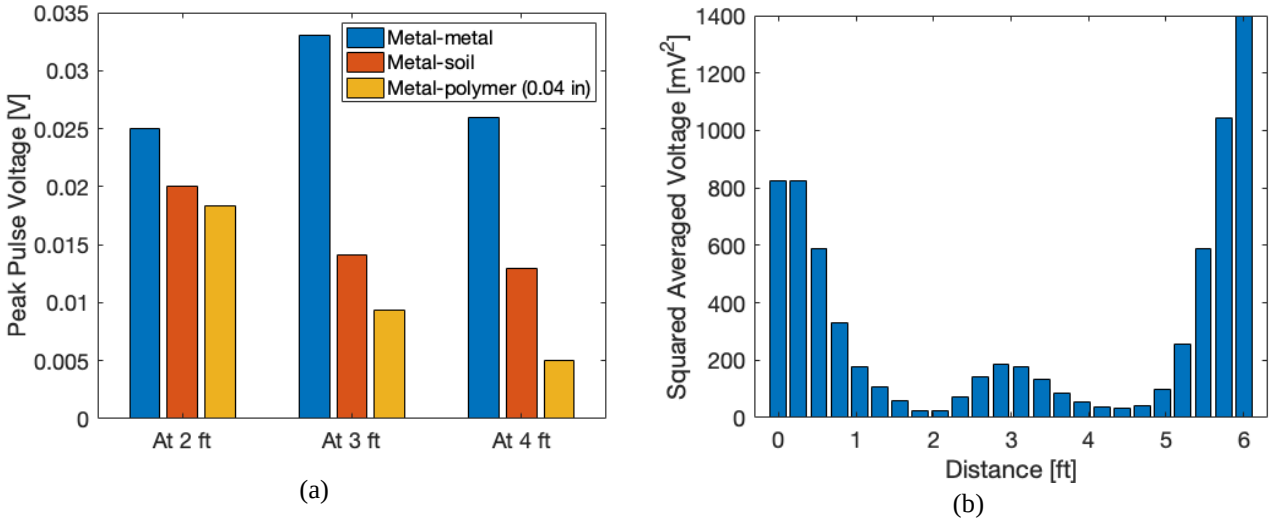

Figure 10. (a) A comparison of return wave packet peak-voltages at various locations shows a reduction in return wave-packet energy when reflected from less stiff interfaces, even as applied pressure remains constant. (b) The averaged response voltage when the pressurized soil was at the 3-foot position shows a notable peak during the 3 ft window. The response voltage was averaged in windows corresponding to 0.25 ft length increments and was then squared to exaggerate the peaks and dips.

The peak response pulse at different locations was compared between material interfaces, as shown in Fig. 10a. Responses were only compared at 2, 3, and 4 ft pressure locations, because no response was observed for the other locations during metal-polymer interface testing. It should be noted that there is a potential bias in comparing peak reflected response voltages due to any loss of energy that may have occurred from debonding. However, the weakest overall response occurred during Dragon Skin testing, which took place before the metal-soil interface tests. This means that, even in the presence of potential worsening debonding, a stronger residual signal was generated from the soil interface than when using Dragon Skin. Fig. 10a shows that the metal-metal interface produced the strongest response, followed by the metal-soil interface and the metal-polymer producing the lowest, level of response.

In addition, the squared averaged voltage response over the entire length of the aluminum strip when the pressurized soil interface was placed at the 3 ft position is shown in Fig. 10b. The response voltage was averaged in windows corresponding to 0.25 ft length increments and was then squared to exaggerate the peaks and troughs. It can be seen from Fig. 10b that a localized peak occurred near the 3 ft position, which corresponded to the location of the metal-soil interface. Through this simple processing technique, the relative location of the pressurized soil could be determined through UTDR. These initial results indicate that it may be possible to use UTDR to detect a metal-soil interface for the purposes of scour monitoring.

4. CONCLUSIONS

Local scour is one of the most pressing issues facing overwater infrastructure systems worldwide. While there are techniques that can successfully detect scour on a periodic basis, new monitoring methods are still needed to monitor scour and capture scour depth during extreme events. Thus, the objective of this work was to investigate the potential of using UTDR for scour depth monitoring in a controlled and dry laboratory setting. Lamb waves were introduced into a 6 ft aluminum strip using an MFC. When applied pressure was introduced onto the surface of an aluminum strip with a metal-to-metal interface, a reflected wave was produced and could be detected by an MFC sensor. The position of the reflected wave packet, which was determined using wave speed and time-of-flight, was found to be consistent with the location of the applied pressure interface. The amount of reflected energy also correlated well with the magnitude of pressure applied strip. Furthermore, there were notable changes in the amount of reflected energy when the type of pressure interface was varied. Testing performed with metal-polymer interface showed a very low reflective response, while a metal-soil interface showed an intermediate response. These tests successfully showed that the propagating Lamb wave interacted with the applied pressure at different locations along the aluminum strip. In addition, the propagating Lamb waves reflected more or less energy depending on the material interface where pressure was applied. Although further study is needed, the return

wave packets appearing from the metal-soil interface testing suggest the plausibility of using UTDR to detect a soil interface for the purposes of scour monitoring.

ACKNOWLEDGEMENTS

This project was funded by the U.S. Army Corps of Engineers (USACE) under cooperative research agreement no. W912HZ-17-2-0024. The authors gratefully acknowledge the collaboration of Dr. A. Drew Barnett and Dr. Joey Reed from Elintrix.

REFERENCES

[1] Montalvo, C., Cook, W. and Keeney, T., "Retrospective analysis of hydraulic bridge collapse," J. Perform. Constr. Facil. **34**(1), 2–9 (2020).

[2] Arneson, L. A., Zevenbergen, L. W., Lagasse, P. F. and Clopper, P. E., "Evaluating scour at bridges. HEC-18. Fifth Edition, Hydraulic Engineering Circular No. 18. Publication," No. FHWA-HIF-12-003. U.S. Dep. Transp. Fed. Highw. Adm.(18), 340 (2012).

[3] American Association of State Highway and Transportation Officals., "AASHTO LRFD bridge design specifications" (2010).

[4] Melville, B. W., "Local scour at bridge sites" (1975).

[5] Pizarro, Manfreda and Tubaldi., "The Science behind Scour at Bridge Foundations: A Review," Water **12**(2), 374 (2020).

[6] Yao, C., Darby, C., Hurlebaus, S., Price, G. R., Sharma, H., Hunt, B. E., Yu, O. Y., Chang, K. A. and Briaud, J. L., "Scour monitoring development for two bridges in Texas," Geotech. Spec. Publ.(210 GSP), 958–967 (2010).

[7] De Falco, F. and Mele, R., "The monitoring of bridges for scour by sonar and sedimetri," NDT E Int. **35**(2), 117–123 (2002).

[8] Richardson, E. V. and Richardson, J. R., "Bridge scour" (1989).

[9] Lin, Y. Bin, Chen, J. C., Chang, K. C., Chern, J. C. and Lai, J. S., "Real-time monitoring of local scour by using fiber Bragg grating sensors," Smart Mater. Struct. **14**(4), 664–670 (2005).

[10] Huang, L., Wang, D. and Zhou, Z., "A new type of optical FBG-based scour monitoring sensor," 103–109 (2007).

[11] Kong, X., Ho, S. C. M., Song, G. and Cai, C. S., "Scour monitoring system using fiber Bragg grating sensors and water-swellable polymers," J. Bridg. Eng. **22**(7), 1–11 (2017).

[12] Ding, Y., Yao, Q., Zhang, Z., Wang, X., Yan, T., Yang, Y. and Lv, H., "A new method for scour monitoring based on fiber Bragg grating," Meas. J. Int. Meas. Confed. **127**(May 2017), 431–435 (2018).

[13] Zarafshan, A., Iranmanesh, A. and Ansari, F., "Vibration-based method and sensor for monitoring of bridge scour," J. Bridg. Eng. **17**(6), 829–838 (2012).

[14] Azhari, F. and Loh, K. J., "Laboratory validation of buried piezoelectric scour sensing rods," Struct. Control Heal. Monit. **24**(9), 1–14 (2017).

[15] Funderburk, M. L., Huang, S.-K., Loh, C.-H. and Loh, K. J., "Densely distributed and real-time scour hole monitoring using piezoelectric rod sensors," Adv. Struct. Eng. **22**(16), 3395–3411 (2019).

[16] Yankielun, N. E. and Zabilansky, L., "Laboratory investigation of time-domain reflectometry system for monitoring bridge scour," 1279–1284 (1999).

[17] Yu, X. and Yu, X., "Laboratory evaluation of time-domain reflectometry for bridge scour measurement: Comparison with the ultrasonic method," Adv. Civ. Eng. **2010** (2010).

[18] Yu, X. and Yu, X., "Time domain reflectometry automatic bridge scour measurement system: Principles and potentials," Struct. Heal. Monit. **8**(6), 463–476 (2009).

[19] Yu, J. D., Lee, J. S. and Yoon, H. K., "Circular time-domain reflectometry system for monitoring bridge scour depth," Mar. Georesources Geotechnol. **38**(3), 312–321 (2020).

[20] Wang, K., Lin, C. P. and Chung, C. C., "A bundled time domain reflectometry-based sensing cable for monitoring of bridge scour," Struct. Control Heal. Monit. **26**(5), 1–14 (2019).

[21] Wang, K. and Lin, C. P., "Applicability and limitations of time domain reflectometry bridge scour monitoring system in general field conditions," Struct. Heal. Monit. (2020).

[22] Munian, R. K., Mahapatra, D. R. and Gopalakrishnan, S., "Lamb wave interaction with composite delamination," Compos. Struct. **206**(April), 484–498 (2018).

[23] Zhao, J., Durham, N., Abdel-Hadi, K., McKenzie, C. A. and Thomson, D. J., “Acoustic guided wave techniques for detecting corrosion damage of electrical grounding rods,” Meas. J. Int. Meas. Confed. **147**, 106858 (2019).
[24] An, Y. K., Kim, J. H. and Yim, H. J., “Lamb wave line sensing for crack detection in a welded stiffener,” Sensors (Switzerland) **14**(7), 12871–12884 (2014).
[25] Rathod, V. T., Mahapatra, D. R., Jain, A. and Gayathri, A., “Characterization of a large-area PVDF thin film for electro-mechanical and ultrasonic sensing applications,” Sensors Actuators, A Phys. **163**(1), 164–171 (2010).
[26] Alleyne, D. N. and Cawley, P., “The interaction of lamb waves with defects,” IEEE Trans. Ultrason. Ferroelectr. Freq. Control **39**(3), 381–397 (1992).
[27] Alleyne, D. N. and Cawley, P., “Optimization of lamb wave inspection techniques,” NDT E Int. **25**(1), 11–22 (1992).
[28] Sodano, H. A., Park, G. and Inman, D. J., “An investigation into the performance of macro-fiber composites for sensing and structural vibration applications,” Mech. Syst. Signal Process. **18**(3), 683–697 (2004).
[29] Mańka, M., Rosiek, M., Martowicz, A., Stepinski, T. and Uhl, T., “Lamb wave transducers made of piezoelectric macro-fiber composite,” Struct. Control Heal. Monit. (2013).
[30] Kundu, T. and Maslov, K., “Material interface inspection by Lamb waves,” Int. J. Solids Struct. **34**(29), 3885–3901 (1997).